Machinable, High-Conductivity NaSICON through Mitigation of Humidity Effects during Solid-State Synthesis

*Amanda S. Peretti, Erik D. Spoerke, Michael E. Ureña, Isaac D. Dyer, Perla A. Salinas, Mark. A. Rodriguez, Philip S. Mantos, John N. Williard, and Leo J. Small**

Sandia National Laboratories, Albuquerque, NM USA 87185

*E-mail: ljsmall@sandia.gov, Phone: +1 505 844 9987

KEYWORDS

NaSICON, sodium, ion conductor, solid state electrolyte, ceramic, processing, humidity

ABSTRACT

The Na^+ super ion conductor (NaSICON, $Na_{1+x}Zr_2Si_xP_{3-x}O_{12}$) is a solid electrolyte well-known for fast, selective Na^+ transport at low temperatures, uniquely enabling sodium-based batteries. Producing high-quality NaSICON from solid-state methods, especially when cost-effective, potentially hygroscopic precursors are used, is not trivial. To understand and eliminate the influence of humidity during processing, a scheme was developed to reproducibly yield a high Na^+ conductivity (3.75 mS cm^{-1} at 25 °C, 81.7 mS cm^{-1} at 150 °C), high density (97%), and machinable NaSICON without the use of binders, sintering aids, or dopants. Controlled humidity studies over 20-50% RH coupled with thermal, structural, and electrical analysis reveal that calcination

temperatures <1000 °C leave NaSICON processing susceptible to water absorption at >20% RH due to the presence of hygroscopic Na_3PO_4 and Na_2CO_3 during shaping, pressing, and sintering. Water absorption results in NaSICON with lower densities, machinability, and Na^+ conductivity, due to impaired intergranular Na^+ transport. At the other extreme, fully converting precursor to the NaSICON phase at 1230 °C before pressing and sintering leads to poor conductivity and density. By calcining at 1000 °C, excellent quality NaSICON may be produced under a range of laboratory environments, enabling low-cost production of high-conductivity, machinable NaSICON necessary the ever-growing energy storage market.

INTRODUCTION

The sodium super ion conductor (NaSICON) is a solid state electrolyte first reported by Goodenough and Hong in 1976.[1] Nominally $Na_{1+x}Zr_2Si_xP_{3-x}O_{12}$, NaSICON comprises a family of ceramics consisting of ZrO_6 octahedra coordinated to SiO_4 and PO_4 tetrahedra.[2, 3] The resulting structure creates high-conductivity Na^+ channels and enables unusually high room temperature solid-state sodium ion conductivities as high as 4 mS cm^{-1}.[4]

Though NaSICON has found applications in chemical separations[5, 6] and even gas sensing,[7] NaSICON research has surged in recent years, propelled by the demand for energy storage technologies beyond traditional Li-ion batteries.[8, 9] Indeed NaSICON has been integrated into molten sodium batteries,[10, 11, 12, 13, 14] solid-state batteries,[9, 15, 16] and even less-conventional sodium batteries.[17] For most applications there are several key properties that impact performance including ionic conductivity and (less commonly discussed) mechanical integrity, each of which is a function of NaSICON phase chemistry, ceramic density, and defects (pinholes, cracks, etc.) A variety of synthetic methods have been developed to optimize NaSICON performance, including

traditional solid-state ceramic processing,[1, 13, 18, 19] sol-gel methods,[4, 19, 20, 21] spark plasma sintering,[22] and others.[23] Recently, Sakamoto's group demonstrated that hot pressing could be used to create NaSICON with room temperature conductivity near 4.2 mS cm^{-1}, due in part to stresses applied during processing.[24]

One of the major challenges to these approaches is to use scalable starting materials that do not require extremely high processing or sintering temperatures (e.g., >1300 ºC), and that are not hazardous to use (e.g., nitrates or P_2O_5).[20, 25, 26] High temperature processing can be associated with non-uniform diffusion and increased sodium or phosphorus volatility,[27] all of which affect phase purity of the NaSICON. Hazardous or expensive reagents naturally impact the scalability of processing.[28] Here, we describe a process that uses low-cost abundant materials and allows for synthesis of high performance NaSICON sintered at only 1230 ºC.

Many groups have also worked to increase the Na^+ conductivity of NaSICON, potentially increasing the efficiency and decreasing the cost of these energy storage technologies. For example, Jolley et al investigated Al^{3+}, Fe^{3+}, Y^{3+}, Co^{2+}, Ni^{2+}, Zn^{2+} demonstrating the influence of ionic radii on NaSICON conductivity.[29] Luo's group, on the other hand, focused on the effect of divalent Mg^{2+} and Ni^{2+} have on the grain boundary conductivity and presence of secondary phases.[30] Others have examined sintering aids such as antimony tin oxide to successfully increase ionic conductivity.[31] A thorough review of these doping efforts has been compiled by Rao, Bharathi and Patro.[25] In general, these doping efforts are aimed that tuning the size of the "bottleneck" in the NaSICON crystal structure, thus increasing the Na^+ conductivity through the crystalline NaSICON phase. Due to the desired ionic radii, however, expensive rare earth elements such as Sc^{3+} and Y^{3+} are often favored. While intriguing from a science perspective, these elements have the potential to significantly increase the price of NaSICON without commensurate

improvements in NaSICON properties. In contrast, we have found that optimization of the base NaSICON composition combined with optimized standard ceramic processing can yield a higher conductivity NaSICON.

Despite the myriad reports on NaSICON and its high Na^+ conductivity, sintered NaSICON forms are not widely commercially available as commodities today, with only powders being available from select suppliers. NaSICON powders, however, are not suitable starting material for forming solid bodies (pellets, tubes, etc.) of NaSICON, as will be shown later. Forming dense, sintered parts from NaSICON powders, however, can be expensive and technical challenging; the high melting temperature of NaSICON[32] necessitates multiple high temperature processing steps or complex synthesis configurations, limits densification, and complicates ceramic composition due to sodium and phosphate volatility. More commonly, NaSICON parts are synthesized through reactive sintering, where component reagent starting materials react (often through vapor-phase or liquid-phase mass transport) to form the NaSICON phase during relatively cooler sintering/densification thermal treatment.[20, 33, 34] We posit that the dearth of NaSICON parts broadly available to the research community is related to variability in its manufacture. In many reports, statistics around effective NaSICON yield are not provided, and it is not clear if the presented results represent a "hero" sample, or if the method routinely produces high-quality, pinhole-free material able to be subsequently shaped or formed. Our synthetic route employs standard ceramic processing techniques and specifically uses inexpensive, widely available materials – Na_2CO_3 (washing soda), Na_3PO_4 (colloquially "TSP," a cleaning agent), SiO_2 (amorphous silica), and $ZrSiO_4$ (a widely-used opacifier in ceramic glazes).

Equally important, it is demonstrated that typical laboratory humidities (50% RH) can absolutely ruin the quality of NaSICON due to the hygroscopic nature of the precursor materials

and its influence on the reactive sintering process. In these cases, Na^+ conductivity and density can be measured, and phase purity can be demonstrated in XRD, yet yields are abysmal and parts crumble upon being machined. Fortunately, this humidity effect can be largely eliminated through the use of specific calcination temperatures, enabling application of this synthetic route over varying humidities. Herein, complementary electrical, thermal, structural, and microstructural analyses relate the quality of NaSICON cylinders made on 100 g scale, and these parameters are related to the machineability and yield of the formed NaSICON parts.

EXPERIMENTAL

Materials. Na_3PO_4•$12H_2O$ (>98%), and SiO_2 (325 mesh, 99.5%), were purchased from Sigma-Aldrich. Na_2CO_3 (anhydrous, ≥99.5%), $ZrSiO_4$ and $Mg(NO_3)_2 \cdot 6H_2O$ (98-102%) were obtained from Thermo Fisher Scientific. Ethanol (200 proof) was procured from Pharmco. Deionized water was purified to 18.2 MΩ*cm.

NaSICON synthesis was performed at 100 g scale using standard solid-state ceramic processing techniques, outlined in **Scheme 1**. $ZrSiO_4$, Na_3PO_4•$12H_2O$, SiO_2, and Na_2CO_3 powders were combined in a 2:0.6:0.4:0.8 molar ratio (130.59 g total), ball milled overnight using 10 mm cylindrical YSZ milling media in ethanol, and subsequently dried by rotary evaporation before further drying under vacuum overnight. No excess Na source was intentionally added.

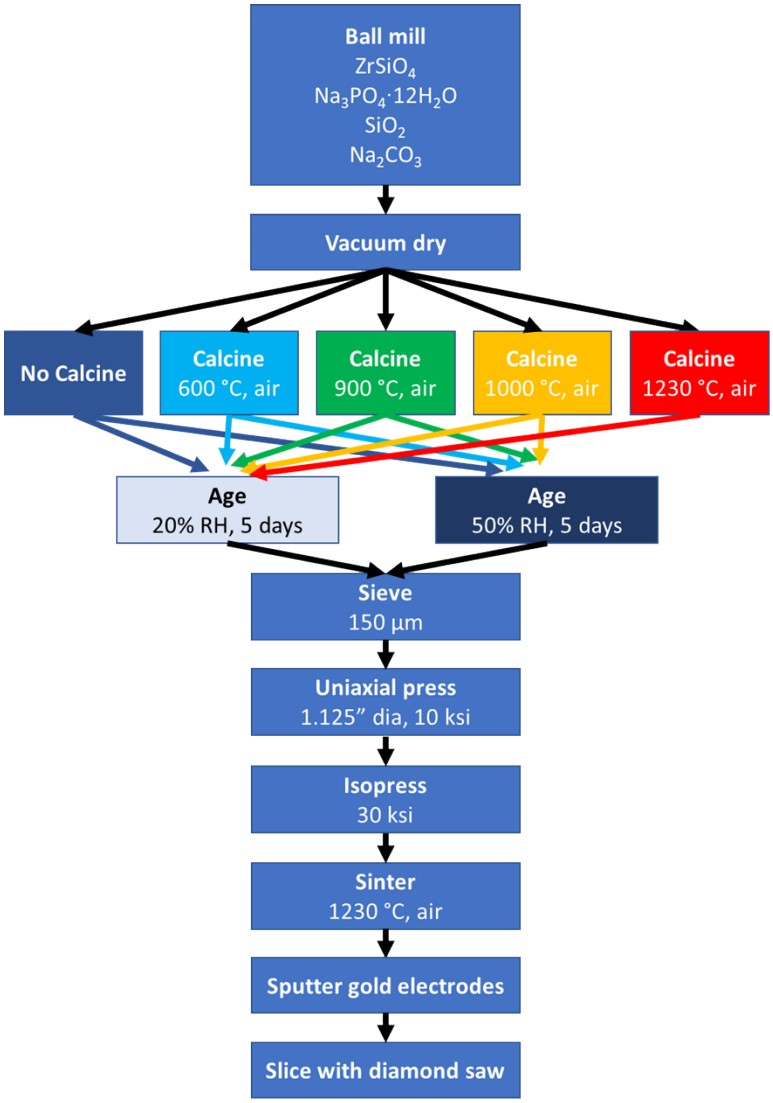

Scheme 1. Flowchart relating NaSICON processing steps used in this work. Calcination and humidity aging steps were varied to understand their influence on the resulting NaSICON discs.

The dried powders were calcined at 600, 900, 1000, or 1230 °C in air for 12 h. A ramp rate of 5 °C min^{-1} was employed for heating, while 10 °C min^{-1} was used for cooling. Additionally, some precursor powder was not calcined, as outlined in Scheme 1.

Afterwards, the precursor powders were aged for 5 days under controlled humidity. A saturated aqueous solution of $Mg(NO_3)_2$ was used to control the humidity inside a 31 L plastic container to 50% relative humidity (RH), and samples kept at 20% RH were left in ambient room humidity closely monitored by hygrometers (NISTtraceable Digi-Sens digital hygrometer and Extech instruments hygrometer).

The aged powders were ground in a mortar and pestle and then manually pressed through a 150 μm sieve. Approximately 20 g was loaded into a 1-1/8" die and uniaxially pressed to 69 MPa (10 ksi), followed by isopressing to 207 MPa (30 ksi).

The pressed cylinder was sintered on a bed of NaSICON precursor powder, covered with an alumina crucible and heated at 5 °C min^{-1} to 1230 °C in air, including holds at 400 °C for 2 h and 600°C for 4 h. The sample was then held at 1230 °C for 12 h before cooling to room temperature at 5 °C min^{-1}. This process yielded a NaSICON cylinder nominally 25 mm in diameter and 20 mm tall. At this point, the density of the NaSICON cylinder was measured by the Archimedes method.

Gold electrodes were sputtered onto opposing ends of the NaSICON cylinders using a Emitech K550X sputter coater. The sidewalls of the cylinder were masked off with Kapton tape and the ends were sputtered until a resistance of < 5.0 Ω across the surface of the electrode was achieved. Na^+ conductivity was then measured, as described later.

The NaSICON cylinder was sliced using a Buehler Isomet High Speed Pro saw. An IsoMet 15LC, 8in [203mm] diamond-coated blade was operated at 4000 rpm and 5 mm min^{-1} feed rate to automatically slice the cylinder into 1 mm thick discs.

Chemical analysis of NaSICON via inductively coupled plasma (ICP) confirmed the target composition for synthesized NaSICON, intended to be nominally $Na_{3.4}Zr_{2.0}Si_{2.4}P_{0.6}O_{12}$.

Values were normalized to Zr, which was added as a single component and is not expected to be volatile during synthesis.

Table 1: Atomic ratios for target composition and synthesized NaSICON determined by ICP. Ratios normalized to non-volatile Zr.

	Na	P	Si	Zr
Target Ratio	3.40	0.600	2.40	2.00
Measured (vs Zr)	3.46	0.620	2.33	2.00

Thermogravimetric Analysis (TGA) and Differential Scanning Calorimetry (DSC) were used to identify mass loss and change in heat flow of NaSICON powders after the aging step in Scheme 1. Thermal analysis was carried out in a Thermogravimetric Analyzer (TGA; NETZSCH STA 409 CD) from room temperature to 1300 °C at a rate of 10 °C min^{-1} under air with a purge flow of 100 mL min^{-1}.

X-ray diffraction (XRD) was performed at room temperature using a Bruker D2 Phaser diffractometer with Cu Kα radiation at an accelerating voltage of 30 kV (10 mA) and 0.2 s integration time. XRD measurements were performed on the starting reagents, after vacuum drying, after calcining/aging, and after sintering.

Temperature-dependent XRD was collected using a Bruker D8 Advance equipped with a sealed tube X-ray source (Cu Kα radiation) operating at 40 kV and 40 mA and a LynxEye XE-T silicon strip detector where patterns were measured in 1D mode. The incident beam employed a 0.6° divergence slit (300 mm goniometer radius) and conventional Bragg-Brentano optics. The diffractometer was configured with an Anton-Paar HTK1600 furnace with a Pt heating strip and samples were run in a static air atmosphere. Prior to the experiment stage temperature was

calibrated by monitoring the thermal expansion of Alumina as determined by heating a 1 cm^2 (0.5 mm thickness) substrate placed directly on the heating stage. The NaSICON precursor sample was placed on top of the same type of alumina substate during the high temperature XRD experiment, and the stage height was adjusted prior to heating based on known XRD peak positions for the initial constituents (e.g., Zircon). Scan parameters for XRD patterns were 10-70° 2q, 0.02° step size, and an equivalent count time of 96 sec/step. The sample was heated at 3 °C/min, dwelling at each 100 °C increment for 1 h before collecting diffraction scans. Each scan required approximately 25 minutes. After reaching the maximum temperature of 1230 °C, the sample was cooled at a rate of 10 °C/min to 50 °C, where the final diffraction pattern was collected. The NaSICON pellet analyzed was made from uncalcined powder equilibriated at 20% RH, uniaxially pressed at 8000 lbs in a 15 mm die for 60 s, and isotatically pressed at 220 MPa for 5 minutes. The resulting pellet was dry polished into a 1 × 1 × 0.05 cm plate using SiC paper.

Na^+ conductivity of the NaSICON cylinder was measured via impedance spectroscopy, after gold sputtering, but before cylinder slicing. A Solartron Analytical 12962A sample holder made contact to the gold-electroded NaSICON cylinder, enabling a Solartron Analytical Modulab MTS to record impedance spectra over 1 MHz – 1 Hz (10 points per decade) at 10 mV_{RMS} AC and 0 V DC. Impedance data were analyzed and equivalent circuits fit using the complex nonlinear least squares algorithm in Z-plot (Scribner Associates, North Pines, NC). To measure Na^+ conductivity at varying temperatures in air, a custom gold-plated stainless steel sample holder was used to contact the gold-electroded NaSICON cylinder. Temperature was controlled by a Tenny TJR thermal chamber. NaSICON was allowed to equilibrate for 3 hours at each temperature before measurements were recorded. Note that cylinders used for Na^+ conductivity analysis were only

lightly polished before being electroded; unlike in other reports, no excessive material removal was performed, due to the uniform nature of the synthesized NaSICON parts.

Scanning electron microscopy (SEM) was used to evaluate the microstructure of NaSICON discs sliced from the sintered cylinder. NaSICON discs were mounted into 1.25" epoxy pucks and then ground using SiC paper at 180 and 600 grit for flatness. Discs were sequentially auto-polished using 9, 6, 3,and 1 μm diamond-based suspensions (Struers) for 5 minutes each at each grit. Finally, discs were vibratory polished for 15 h using 0.04 μm SiO_2. Secondary electron and backscatter electron images were recorded on a JEOL IT800 using a 5 kV accelerating voltage. All samples were coated in AuPd to prevent charging under the electron beam.

Machineability and yield were evaluated after slicing NaSICON cylinders into 1 mm thick discs. Here "machineability" is defined as the number of full NaSICON discs successfully cut from a given cylinder divided by the number of discs expected for a given cylinder height. "Yield" is defined as the number of full NaSICON discs without any defects (pinholes, divots, etc.) divided by the number of 1 mm NaSICON discs expected for a given sintered cylinder height.

RESULTS AND DISCUSSION

Herein is presented the development of a reproducible solid-state, reactive sintering method by which to synthesize high-conductivity, high density, machinable NaSICON (nominally $Na_{3.4}Zr_{2.0}Si_{2.4}P_{0.6}O_{12}$). Of particular interest is the influence of humidity present during processing on the structure and properties of the resulting NaSICON, and how the processing conditions can be optimized to controllably produce high quality NaSICON. Using the typical NaSICON process outlined in Scheme 1, humidity and calcination temperature were systematically varied, and changes in these processing conditions were related to the resulting density, Na^+ conductivity,

machineability, and yield. Changes in these NaSICON properties correlated with (1) water absorption by the precursor powder, as measured by DSC/TGA, (2) controlled development of specific crystalline phases as observed in XRD, and (3) changes in microstructure, specifically grain boundary structure. Together, these structural changes can be related back to electrical properties, implicating differences in Na^+ conduction across grain boundaries as the primary changes in Na^+ conductivity.

Calcination Temperature and Humidity Influence NaSICON Properties

A series of NaSICON cylinders, nominally 25 mm diameter by 20 mm tall were synthesized via the process outlined in Scheme 1, conducted on 100 g scale. After ball milling and drying the starting materials, these precursor powders were aged at either 20% or 50% RH for 5 days in controlled humidity environments. Powders were then either not calcined or calcined at 600, 900, 1000, or 1230 ºC in air. Powders subjected to each of these conditions were then sieved, pressed into cylinders, and sintered in air at 1230 ºC. Repeat cylinders were made for each condition, and for the optimal condition (20% RH, 1000 ºC) 13 cylinders in total were made. The relative densities of the resulting cylinders are presented in **Figure 1A**, assuming a theoretical density of 3.292 g cm^{-3}.[35] For samples aged at 20% RH, increasing the calcination temperature resulted in increased density, until the calcination temperature was increased to 1230 ºC, at which point a significantly lower density was observed. Samples annealed at 50% RH, a similar trend was observed over 600-1000 °C, though at lower densities overall. No density could be measured for samples held at 50% RH that were not calcined, as the cylinders disintegrated during sintering. (See Figure 2). Similarly, the 50% RH, 1230 °C calcine condition was omitted due to poor performance at 20% RH.

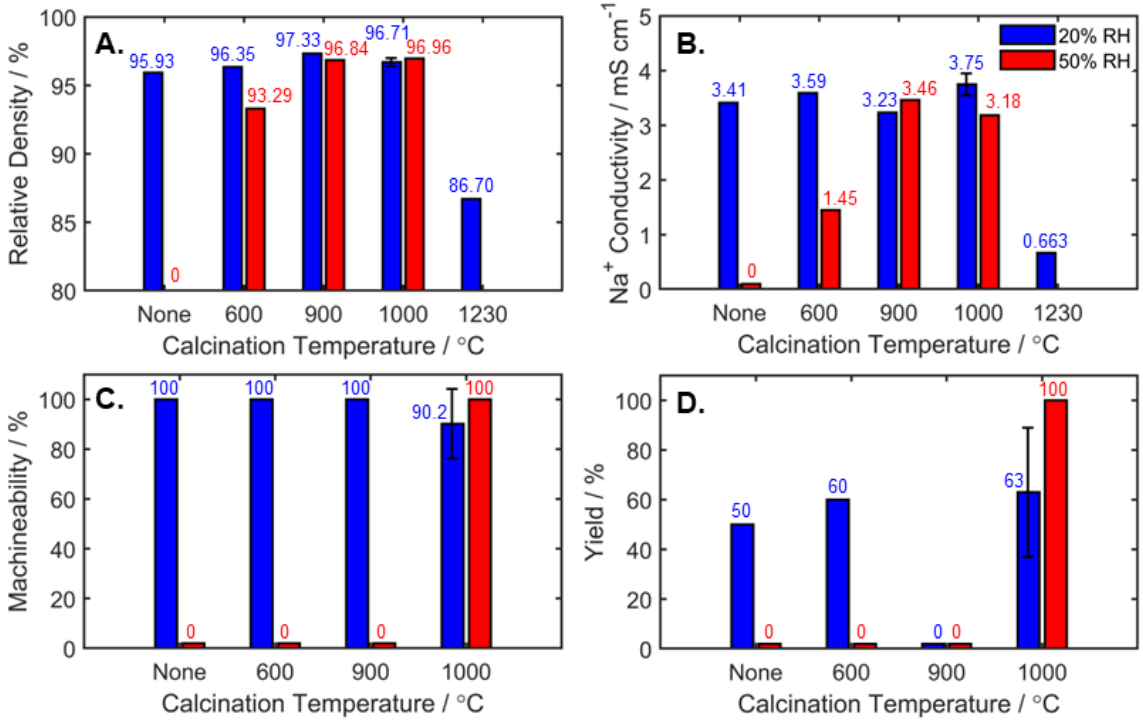

Figure 1. Influence of relative humidity and calcination temperature on (A) relative density, (B) room-temperature Na^+ conductivity, (C) machineability (% discs successfully sliced from cylinder), and (D) yield (% discs without any pinholes). In (A) relative density is plotted as a percentage of theoretical density (3.292 g cm^{-3}).[36, 37]

The NaSICON cylinders were sputtered with Au electrodes, Na^+ conductivity was assessed using impedance spectroscopy and traditional equivalent circuit analysis.[36, 37] The results are summarized in Figure 1B, though detailed results are presented in Figures S1-S3 and Tables S1-S2. At 20% RH, moderate Na^+ conductivities were observed at no calcine, 600, and 900 °C. The highest Na^+ conductivity was recorded at 1000 °C calcination (3.75 ± 0.20 mS cm^{-1}, N=13), while the lowest Na^+ conductivity was recorded at 1230 °C. At 50% RH, no Na^+ conductivity could be recorded for the no calcination samples, and poor (1.45 mS cm^{-1}) Na^+ conductivity was observed at the 600 °C calcination temperature. Increasing to 900 or 1000 °C, however, resulted in respectable Na^+ conductivities of 3.46 and 3.18 mS cm^{-1}. One might have expected that the highest

conductivities would have correlated directly with the highest sample density.[38] The results in Figure 1 show, however, that while densities above 95% are needed to achieve highest conductivities, that the highest densities above this threshold did not necessarily yield the highest conductivities suggests other variables may be impacting performance.

To verify uniform Na^+ conductivity throughout the NaSICON cylinder, all slices of one cylinder made from powder calcined at 1000 °C and aged at 20% RH were evaluated. Na^+ conductivity was 3.63 ± 0.11 mS cm^{-1} (N=6), indicating excellent uniformity. Measurements from individual slices have been compiled in Table S3.

While densities and Na^+ conductivities could be measured for cylinders made using 8 out of the 9 processing conditions, such positive results were not observed during slicing the cylinders into 1 mm thick discs. Beyond traditionally characterized material properties of density and conductivity, two additional, highly important metrics were devised to describe the practical usefulness of the sintered NaSICON (1) machineability and (2) yield. Machineability, shown in **Figure 1C**, relates the number of discs successfully sliced from the cylinder compared to the number expected based on cylinder size (as a percentage). All NaSICON cylinders made at 20% RH exhibited 100% machineability, while at 50% RH only the samples made with 1000 °C withstood slicing. Example photographs relating this behavior are provided in **Figure 2**. Additional photographs of highly-machinable NaSICON processed at 20% RH and 1000 °C calcination are provided in **Figure S4**.

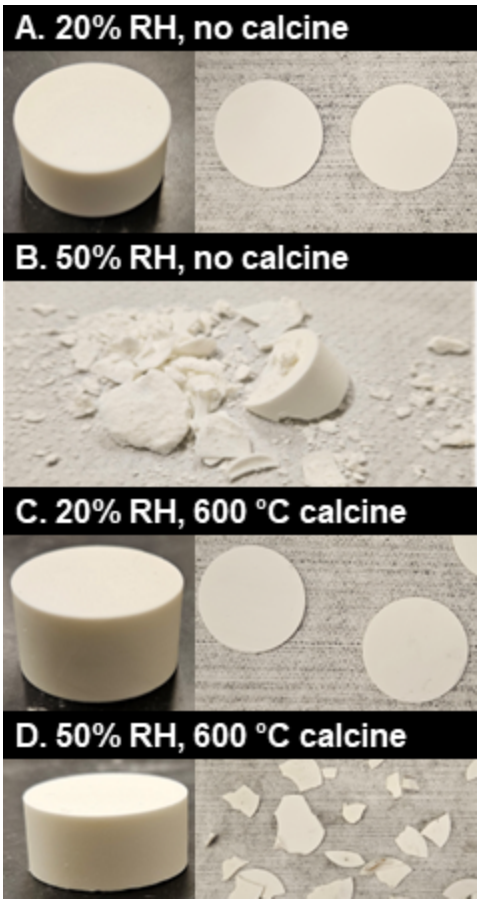

Figure 2. Photographs of NaSICON processed per Scheme 1 using a (A) 20% RH, no calcine, (B) 50% RH, no calcine (cylinder disintegrated during sintering), (C) 20% RH, 600 °C calcine, and (D) 50% RH, 600 °C calcine. Images on left are after sintering while those to the right are of representative discs of the same cylinder after slicing. All cylinders and discs are nominally 25 mm in diameter.

The sliced NaSICON discs were then inspected under 2-5× optical magnification for pinholes or cracks that would preclude their use in a practical device where mechanical integrity is essential. "Yield" in **Figure 1D** describes the number of pinhole-free discs as a percentage of total discs expected from the cylinder. At 20% RH, increased yield was observed for increasing calcination temperature, except for 900 °C, where the cylinders suffered hairline cracks. At 50% RH, only the 1000 °C calcination temperature was machinable, and all discs were pinhole-free (100% yield). Thus, the 1000 °C calcination showed high yields regardless of the humidity at

which the NaSICON precursor was aged. In other qualitative tests to demonstrate machineability, cylinders made using the 1000 °C calcine were successfully ground to shape, while others had cylindrical sections removed via a diamond-coated hole saw in a drill press.

In sum, increasing the calcination temperature generally increased the density until a maximum of about 97.0% (±0.3%) was achieved at 900-1000 ºC. Further increasing the calcination temperature to 1230 °C, a temperature at which the NaSICON phase will begin to crystallize, severely decreased the density. For samples aged at 20% RH, neither the density nor the Na^+ conductivity was profoundly influenced by calcination temperature, though the 1000 °C temperature resulted in by far the highest conductivity. When precursor powders were aged at 50% RH, however, calcination temperatures dramatically affected conductivities and densities with 900 °C and 1000 °C calcinations leading to substantially higher values. Slicing the cylinders into pellets, 20% RH samples were 100% machinable, though increasing calcination temperature led to increased yields. 50% RH samples, on the other hand, showed poor machineability; only at 1000 °C calcination were both 100% machinability and yields observed. On the basis of these properties, the 1000 °C calcination temperature clearly produces the most desirable NaSICON ceramics, minimally influenced by humidity present during synthesis.

Thermal Analysis Reveals Increased Water Uptake at Higher Humidities

To quantify the amount of water absorbed by the NaSICON precursor powders after calcination and aging, DSC/TGA was performed, and the resulting data are plotted in **Figure 3**. For the uncalcined 20% RH sample in Figure 3A, a large endothermic peak, attributed to release of absorbed or adsorbed H_2O, is observed over 20-115 ºC with a peak at 68 °C. This peak is suppressed for powders calcined at 600, 900 or 1000 °C. A corresponding mass loss is simultaneously observed in TGA, with increased calcination temperature resulting in less mass

loss. At 50% RH, the large DSC peak and corresponding mass loss in TGA are observed across all calcination temperatures, though this effect is minimized at higher calcination temperatures. The overall trend in adsorbed (or absorbed) water released (25-150 °C) from the NaSICON precursor powders in summarized in **Figure 4**. Here it is clearly seen that higher calcination temperatures decrease the amount of water absorbed, with the 20% RH, 1000 °C condition retaining 99.9% of its starting mass at 150 °C.

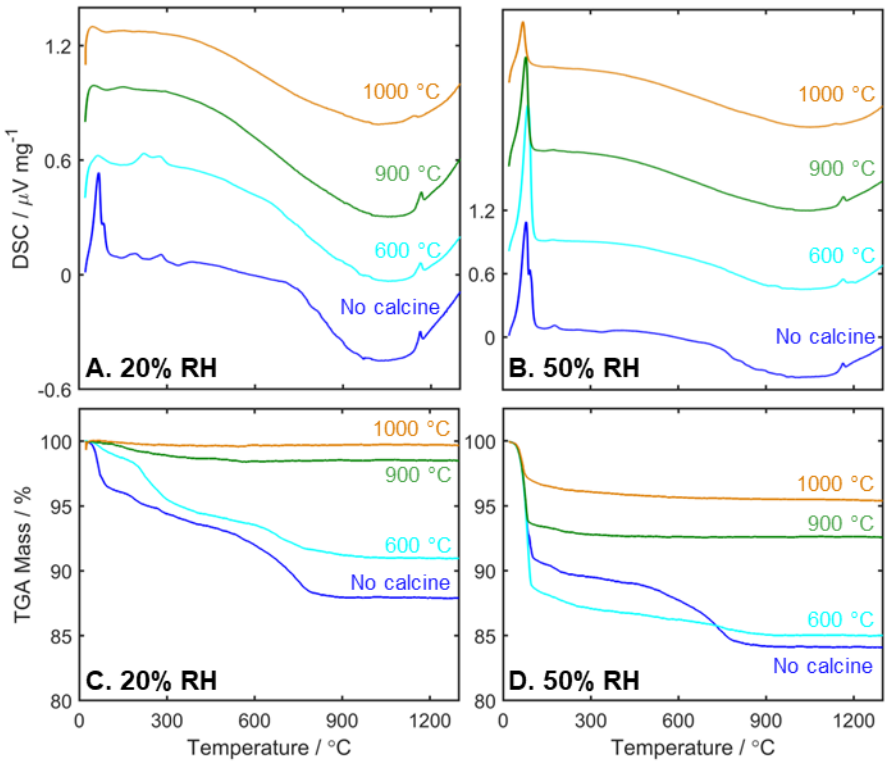

Figure 3. Thermal analysis of NaSICON precursor powders. DSC for precursor powders after calcining at different temperatures and then aging at (A) 20 or (B) 50% RH. Corresponding TGA thermograms for (C) 20% or (D) 50% RH. In DSC, endotherms point upwards.

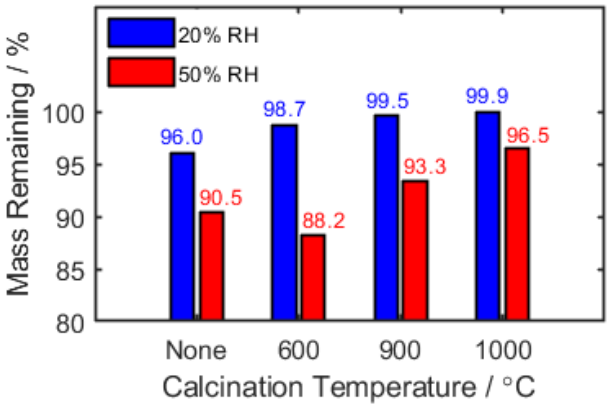

Figure 4. Comparison of the mass of NaSICON precursor powder remaining after heating 25-150 °C during TGA, ascribed to loss of adsorbed or absorbed H_2O.

Beyond 150 °C, some distinct features should also be pointed out in thermal analysis. First, a series of two peaks are observed near 200 and 280 °C for 20% RH samples uncalcined or calcined at 600 °C (**Figure S5**). Samples aged at 50% RH showed only a single peak at 181 °C for the uncalcined sample. These peaks are attributed to phase transitions seen in Na_2CO_3 (**Figure S6B**) and Na_3PO_4 (**Figure S7A**). Additionally, the endothermic peak near 1160 °C is attributed to the formation of an intermediate phase, $Na_2ZrSi_2O_7$. The intensity of this DSC peak is significantly lower for the 1000 ºC calcined powders than powders calcined at other temperatures, suggesting formation of this intermediate phase has already occurred for the 1000 °C calcine samples. Temperature-dependent X-ray diffraction data supporting this phase evolution is presented in Figure S8. Powders that did not display this DSC peak resulted in sintered NaSICON pellets with the best overall properties, suggesting formation of this intermediate phase prior to sintering is beneficial to the resulting NaSICON and its ability to tolerate humidity.

To identify the source of water absorption, the two likely culprits, Na_2CO_3 and $Na_3PO_4{\cdot}12H_2O$, were separately analyzed. Na_2CO_3, purchased anhydrous, retained 99.23% of mass over 25-150 °C, decreasing to 98.45% after aging at 50% RH for 5 days (Figure S6). Beyond

its melting point of 851 °C, Na_2CO_3 was observed to decompose. $Na_3PO_4 \cdot 12H_2O$, on the other hand, retained only 47% of its mass over 25-150 °C, close to the 43% expected from stoichiometry (Figure S7).

From these data, it is hypothesized that Na_2CO_3 and Na_3PO_4 will slowly rehydrate at room temperature even if calcined at 600 °C, when all molecular water is expected to be removed. This effect is exacerbated at higher humidities and, if too much H_2O is absorbed, will negatively influence the properties of the resulting NaSICON (Figure 1). Water absorption > 4 wt% of the total precursor mass results in poor density, conductivity, and machinability. Understanding mechanistically how the water influences the reactive sintering process were the focus of subsequent XRD and SEM studies.

High Temperature Calcines Eliminate Hygroscopic Phases

To positively identify the crystalline phases present during NaSICON processing, XRD was employed both after aging the precursor powder and after sintering NaSICON cylinders made from the same precursor powder.

Characteristic diffraction patterns are plotted in **Figure 5** for NaSICON precursor powders aged at 20% or 50% RH and calcined at varying temperatures. A zoomed-in view of 12-22° 2θ is provided in Figure S9. All starting reagents (Na_2CO_3, $Na_3PO_4 \cdot 12H_2O$, $ZrSiO_4$) except amorphous SiO_2 can be identified in the uncalcined powders (See Figure 5). While the identification of $ZrSiO_4$ and Na_2CO_3 is straightforward, characterization of the Na_3PO_4 phases is more nuanced. The as-received $Na_3PO_4 \cdot 12H_2O$ is identified in XRD as $Na_{6.33}(PO_4)_2(OH)_{0.33}(H_2O)_{24}$, consistent with a <2% NaOH impurity stated in the manufacturer's specification sheet. Upon milling and drying per Scheme 1, the "No calcine" powder aged at 20% RH and plotted in Figure 5A, shows

diffraction peaks characteristic of $ZrSiO_4$, Na_2CO_3, and γ and α-Na_3PO_4. Additionally, a trace HNa_2PO_4 phase may also be present (see Figure S10). That the majority Na_3PO_4 phases identified are anhydrous suggests that the initial ball milling and vacuum drying process (see Scheme 1) largely dehydrated the starting $Na_3PO_4 \cdot 12H_2O$ (Figure S11). The analogous structural change for Na_2CO_3 upon water absorption is more subtle, but closer analysis (Figure S12) is consistent with the small changes observed in TGA (Figure S6).

For the not calcined powders aged at 50% RH, similar phases are identified - $ZrSiO_4$, Na_2CO_3, and γ- and β-Na_3PO_4. Additionally, trace $Na_2(CO_3) \cdot H_2O$ and a more hydrated Na_3PO_4 phase - $Na_4(P_2O_6)(H_2O)_{10}$ - are observed (Figure S13). Overall, the increase in humidity from 20 to 50% RH has resulted in the formation of more hydrated Na_3PO_4 and Na_2CO_3 phases.

Upon increasing the calcination temperature to 600 °C, no significant changes are observed in XRD for the 20% RH case. At 50% RH, the trace $Na_2(CO_3) \cdot H_2O$ phase is no longer observed. Throughout these samples, there is sometimes a difference in the peak intensity at 20.7° (γ-Na_3PO_4), as the ratio of γ- to β-Na_3PO_4 changes with processing temperature.[39] At 900 °C peaks characteristic of the NaSICON structure begin to appear at 13.7° and 19.4° 2θ for both 20 and 50% RH. These peaks grow in intensity at 1000 °C calcination, and peaks over 10-20° 2θ characteristic of hydrated Na_3PO_4 phases disappear for the 50% RH case, leaving only (anhydrous) β and γ-Na_3PO_4 peaks. Upon increasing the calcination temperature to 1230 °C, peaks attributed to $ZrSiO_4$ (20.0, 27.0°) and γ-Na_3PO_4 (20.7°) disappear, and the powder is converted to the monoclinic NaSICON phase. From this analysis it is concluded that a calcination temperature of at least 1000 °C is needed to minimize rehydration of Na_3PO_4 and Na_2CO_3 phases through the *partial* conversion of the powder into NaSICON-like phases.

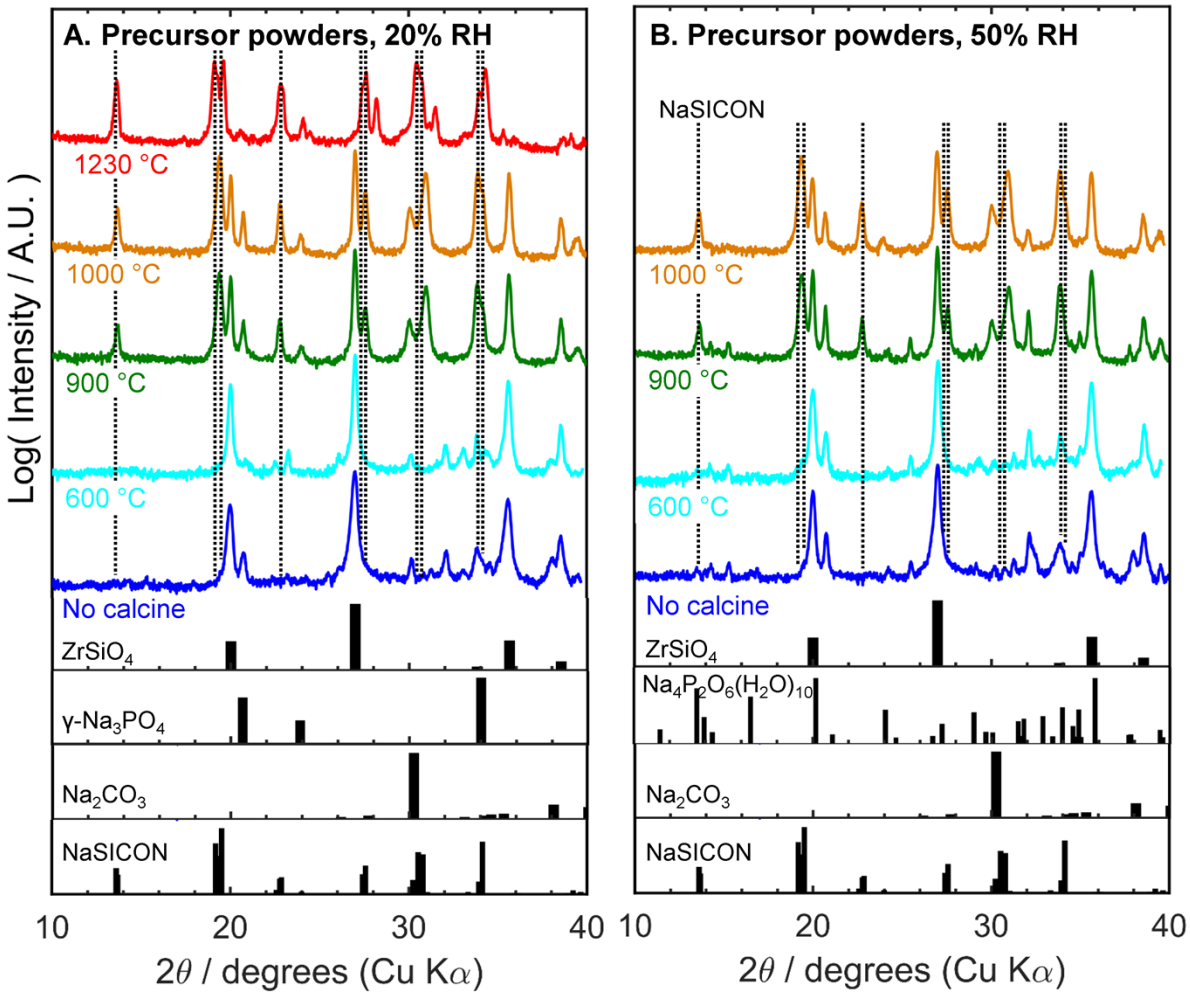

Figure 5. X-ray diffraction patterns for precursor powders not calcined or calcined at 600, 900, 1000, or 1230 °C and then held at (A) 20% RH or (B) 50% RH for 5 days. Reference powder diffraction files for select materials are plotted: $ZrSiO_4$ (PDF 04-009-8352), γ-Na_3PO_4 (PDF 00-030-1233), $Na_4(P_2O_6)(H_2O)_{10}$ (PDF 04-019-4464), Na_2CO_3 (PDF 04-011-4108) and NaSICON (PDF 04-022-0983). Vertical dotted lines reference key NaSICON peak positions.

Examining the sintered pellets in XRD reveals fewer differences, as seen in **Figure 6**. Across all conditions, the monoclinic NaSICON phase is identified, along with a trace ZrO_2 impurity commonly seen in the literature.[19, 20, 40] NaSICON made after aging at 50% RH without calcining displays a peak near 29.5° 2θ, suggesting crystalline SiO_2 is present. XRD patterns for powders calcined at 900 or 1000 ºC appear the same at 20 or 50% RH, consistent with performance

characteristics in Figure 1. Powders calcined at 1230 ºC, however, display subtle differences in XRD patterns compared to those calcined at 1000 ºC. Such differences include the peak spacing of the doublet near 19º 2θ and the shoulders near 30º and 34º 2θ. These changes suggest subtle, undesired, differences in the NaSICON crystal structure arising from the extended time (calcination and sintering) at 1230 ºC. Overall, these results suggest that is it quite "easy" to synthesize the NaSICON crystal phase, but the resulting properties may vary considerably, despite the overwhelming presence of the NaSICON phase in XRD.

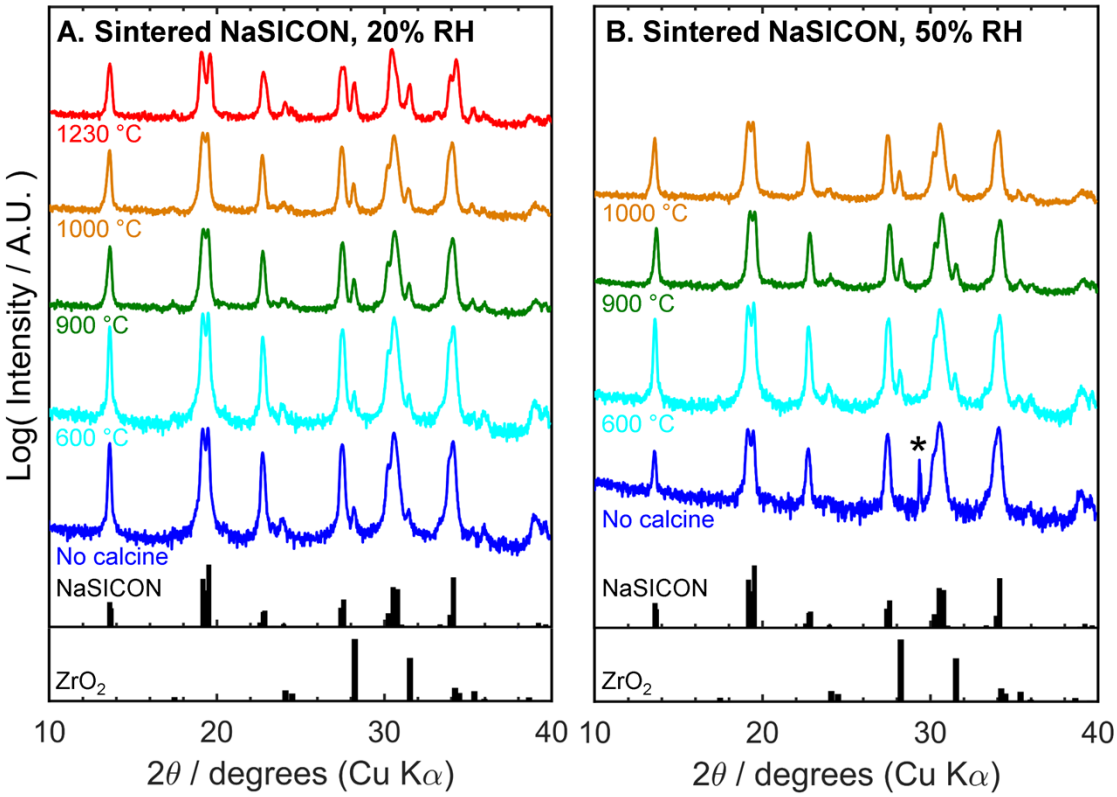

Figure 6. X-ray diffraction patterns for sintered NaSICON cylinders made using powders not calcined or calcined at 600, 900, 1000, or 1230 °C and then held at (A) 20% RH or (B) 50% RH for 5 days before sintering. The asterisk (*) in (B) denotes a peak attributed to SiO_2. Reference powder diffraction files are plotted at bottom for NaSICON (PDF 04-022-0983) and ZrO_2 (PDF 04-002-8305).

Humidity and Calcination Temperature Control Influence Microstructure

To understand the influence of the processing conditions on the resulting NaSICON ceramic microstructure and any possible non-crystalline phases, pellets sliced from sintered NaSICON were polished and examined in SEM. Representative micrographs are provided for select processing conditions in Figure 7. Backscattered electron imaging is used in these micrographs to enhance contrast between the NaSICON phase and any lower density intergranular glassy phases.[10] In these images, the intergranular phase appears as small dark regions; this is not porosity. A comparison of SEM images simultaneously recorded using secondary and backscattered images is presented in Figure S14 to highlight the differences. Bright spots are attributed to a minor ZrO_2 phase, seen in the XRD analysis (Fig. 6) and throughout the literature.[2, 10, 20, 22] Throughout nearly all processing conditions, cuboid NaSICON grains on the order of 1 μm are observed. For samples calcined at 1000 °C and aged at 20% RH, clusters of 3-4 NaSICON grains about 10 μm in total size are occasionally seen (~5 clusters per 12,000 μm^2), shown in the top left of Fig. 7E. No glassy phase is seen between these clustered grains, and EDS mapping (Figure S15) shows that they are compositionally indistinguishable from the rest of the NaSICON microstructure (i.e. not a secondary phase). The formation of these larger grained clusters appears to have been promoted by the 1000 °C calcination temperature and partial formation of an intermediate NaSICON phase prior to sintering.

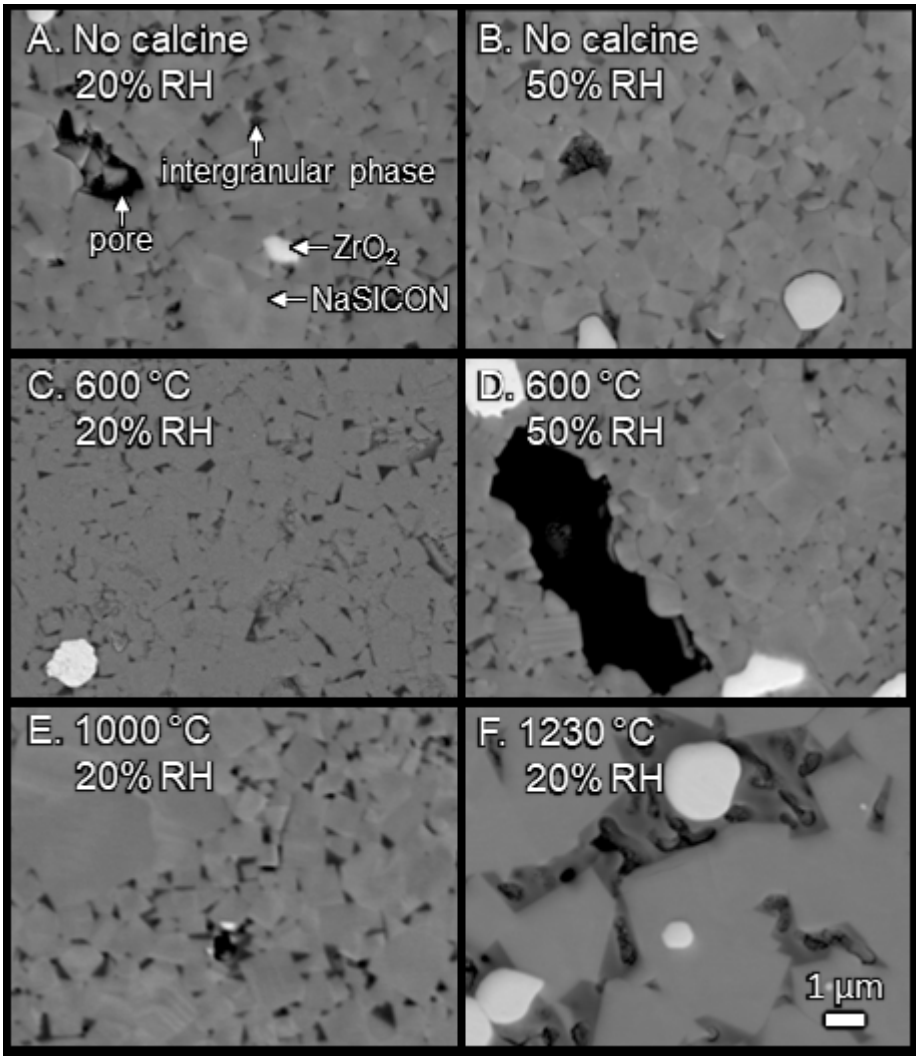

Figure 7. Backscatter SEM micrographs of sintered NaSICON pellets made from precursor powders calcined at various temperatures and then aged at 20 or 50% RH. (A) No calcine, 20% RH, (B) No calcine 50% RH (disintegrated, mounted in epoxy to stabilize), (C) 600 °C, 20% RH, (D) 600 °C, 50% RH, (E) 1000 °C, 20% RH, (F) 1230 °C, 20% RH. All micrographs share the same scale bar.

For the 1230 °C calcination, a markedly different microstructure is observed. Here significantly larger NaSICON grains are observed, along with a significantly larger glassy intergranular phase that does not completely span the space between adjacent grains. Rather, large voids are present between grains. This result is not unexpected, as both the calcination and sintering temperatures were above the crystallization temperature of NaSICON, providing more

time at higher temperature than all other samples and encouraging grain growth. Moreover, this poor intergranular connection is consistent with the low density, poor mechanical properties, and 0% sample yield (excessive pinholes). The lack of reactive sintering is likely responsible for the poor intergranular connection. Unlike powders calcined at lower temperatures, the powder calcined at 1230 °C is largely converted to the NaSICON phase (Figure 5); little of the starting reagents remain and the chemistry present during sintering is fundamentally different.

Interestingly, when no calcine was used, or at 600 °C and 50% RH, significant porosity was observed in SEM (especially, Fig. 7D), correlating strongly with the lower densities (<96%) of these samples. For no calcine, 50% RH, the sample disintegrated during sintering and had to be mounted in epoxy for SEM imaging. These processing conditions correlate to those with some of the highest mass lost upon heating during "sintering" in TGA (Fig. 4), and the lowest machineability and yield (Fig. 1). This porosity was also accompanied by a finely-grained phase collected inside the pores, depicted in further detail in Figure S16. It is hypothesized that the excess water absorbed under these processing conditions altered the nucleation and growth of the NaSICON phase. Generally, the existence of this fine grain phase correlated with lower ionic conductivity (Figure 1).

Image analysis was used to quantify the area percentage of each phase – NaSICON, intergranular glassy phase, ZrO_2, and porosity – and the results are compiled in Table 1. For samples with relatively low porosity (0.0% in Table 1), a positive correlation is seen between processing conditions with higher ionic conductivity and a greater relative fraction of crystalline NaSICON phase. The processing conditions with the highest ionic conductivities also exhibit the lowest relative fractions of intergranular phase and ZrO_2 (and porosity). Combined with DSC and XRD analysis, it is seen that the 1000 °C calcination temperature enables low water adsorption,

partial conversion to crystalline NaSICON, and formation of the intermediate $Na_2ZrSi_2O_7$ phase. These conditions are thought to increase the relative amount of crystalline NaSICON phase and decrease the amount of ZrO_2 present in the final sintered NaSICON ceramic.

Table 1. Quantification of the relative fraction of each phase present in the SEM images.

RH / %	Calcination Temperature / °C	area% NaSICON	area% Intergranular Phase	area% ZrO_2	area% Porosity
20	none	82.6	16.0	1.4	0.0
20	600	82.1	16.5	1.4	0.0
20	900	79.7	18.8	1.5	0.0
20	1000	85.0	14.1	0.9	0.0
20	1230	65.3	24.6	6.6	3.5
50	none	80.5	14.2	2.1	3.2
50	600	82.3	11.9	2.6	3.2
50	900	82.3	16.3	1.4	0.0
50	1000	83.0	14.8	2.2	0.0

Intergranular Na^+ Transport Is Hindered by Water Adsorption after Calcination

To further elucidate the relationship between water absorption during processing and the evolution of the resulting NaSICON microstructures, the impedance spectra from all NaSICON cylinders were analyzed in more detail. Specifically, Na^+ conductivity contributions from bulk crystalline grains were differentiated from Na^+ conduction through the grain boundary phase via equivalent circuit fits (Figure S1, Tables S1-2). Analysis of this data, plotted in Figure 8, demonstrates that as the total Na^+ conductivity ($\frac{1}{\sigma_{total}} = \frac{1}{\sigma_{grain}} + \frac{1}{\sigma_{g.b.}}$) increases, the grain boundary Na^+ conductivity rapidly increases, much faster than the grain conductivity does. Put another way, samples with poor total Na^+ conductivity are strongly affected by poor Na^+ conductivity in grain boundaries. This poor Na^+ connectivity between grains is detrimental to overall Na^+ conductivity,

and correlates strongly with poor microstructure – either the presence of finely-grained phase and microporosity (no calcine or 600 °C 50% RH) or exceptionally large grains poorly connected by the grain boundary phase (1230 °C, 20% RH). Thus, controlling water absorption in NaSICON precursor powder during processing is essential to obtain the idealized microstructure of tightly fitting NaSICON grains, with a small, highly conductive grain boundary phase connecting the grains.

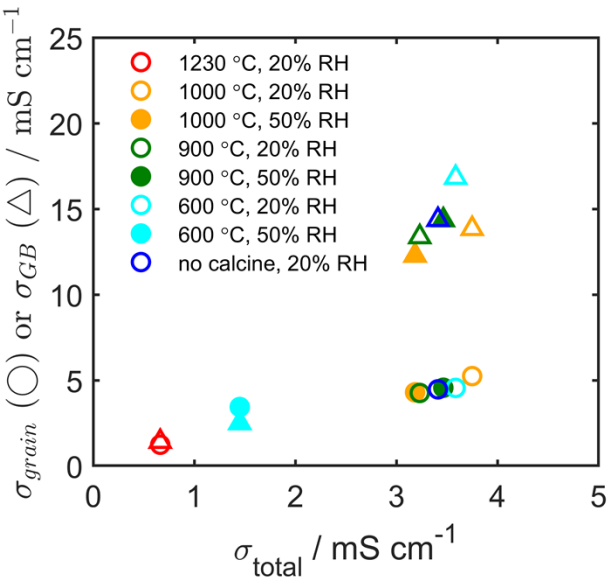

Figure 8. Na^+ conductivity (σ_{grain}) through grains (circles) and grain boundaries ((σ_{GB}, triangles) of NaSICON cylinders made from powders aged at 20% RH (open symbols) or 50% (filled symbols).

CONCLUSION

A solid-state synthetic method for processing high density, high Na^+ conductivity, machinable NaSICON was presented. The process uses widely-available reagents and standard ceramic processing techniques, avoiding binders or costly dopants. Conducted on 100 g scale, clear reproducibility was demonstrated of machined discs with Na^+ conductivity at room

temperature of 3.75 ± 0.20 mS cm^{-1} (81.7 mS cm^{-1} at 150 °C). The calcination temperature was optimized to minimize the effects of humidity on the precursor materials and associated processing conditions. While density and Na^+ conductivity could be measured under many processing conditions, there were considerable differences in the machineability or yield of the material, with high humidities during processing resulting in samples that proved more challenging. By calcining at 1000 °C, partial Na_2CO_3 decomposition was achieved, along with crystallization of a NaSICON-like intermediate phase, dehydrating and decreasing the amount of hygroscopic Na_3PO_4 present. Using this calcination temperature, similar quality NaSICON was achieved at 20% and 50% RH. In fact, the highest Na^+ conductivity NaSICON was produced at 20% RH and 1000 °C calcine. On the other hand, fully converting all starting materials to the NaSICON phase at 1230 °C and using this powder to create a sintered NaSICON body leads to poor conductivity and density. *Partial* conversion of the NaSICON phase during calcination and creation of an intermediate $Na_2ZrSi_2O_7$ phase appears to have led to greatest ceramic performance in the sintered parts.

Differences in Na^+ conductivity were predominantly due to differences in Na^+ conductivity across grain boundaries, as determined by impedance spectroscopy. These differences were corroborated by SEM where significant porosity lined with a fine-grained secondary phase were observed at low calcination temperatures and high humidity. At the highest calcination temperature, 1230 °C, NaSICON grain sizes were significantly larger, yet not poorly connected by the grain boundary phase. These results are consistent with the similarity amongst XRD patterns for sintered NaSICON samples (Figure 6) and highlights the importance of the glassy grain boundary phase in controlling the Na^+ conductivity of the overall NaSICON material. Decreasing the amount of gaseous phases, especially H_2O, present during sintering lead to higher densities and better grain boundary Na^+ conductivity.

With this optimized process, it is envisioned that high-conductivity NaSICON may be more easily synthesized across research groups, or even manufacturers looking to supply the energy storage community with a high conductivity Na^+ separator. Future work is focused on casting the humidity-stable precursor powder into a variety of industrially-relevant shapes.

ASSOCIATED CONTENT

Supporting Information. Nyquist plots of EIS data, detailed fitting parameters and uncertainties of EIS data for calculating Na^+ conductivities, additional photographs of sliced NaSICON, thermal analysis of starting reagents, and XRD patterns for starting reagents.

AUTHOR INFORMATION

Corresponding Author

*Leo J. Small, E-mail: ljsmall@sandia.gov, Phone: +1 505 844 9987

Author Contributions

The manuscript was written through contributions of all authors. All authors have given approval to the final version of the manuscript.

ACKNOWLEDGMENTS

The authors thank S.J. Percival for helpful technical discussions, and V. Perez, and A. Hickman for polishing NaSICON prior to SEM. This material is based upon work supported by the U.S. Department of Energy, Office of Electricity (OE), Energy Storage Division. Sandia National Laboratories is a multi-mission laboratory managed and operated by National Technology and

Engineering Solutions of Sandia, LLC, a wholly-owned subsidiary of Honeywell International, Inc., for the U.S. Department of Energy's National Nuclear Security Administration under contract DE-NA0003525. This written work is authored by an employee of NTESS. The employee, not NTESS, owns the right, title, and interest in and to the written work and is responsible for its contents. Any subjective views or opinions that might be expressed in the paper do not necessarily represent the views of the U.S. Department of Energy or the United States Government. The publisher acknowledges that the US Government retains a non-exclusive, paid-up, irrevocable, world-wide license to publish or reproduce the published form of this written work or allow others to do so, for US Government purposes. The DOE will provide public access to results of federally sponsored research in accordance with the DOE Public Access Plan.

REFERENCES

1. J. B. Goodenough, H. Y.-P. Hong, and J. A. Kafalas, "Fast Na+-ion Transport in Skeleton Structure," *Mat. Res. Bull.,* 11 203-20 (1976).
2. A. G. Jolley, D. D. Taylor, N. J. Schreiber, and E. D. Wachsman, "Structural Investigation of Monoclinic-Rhombohedral Phase Transition in $Na_3Zr_2Si_2PO_{12}$ and Doped NASICON," *J. Am. Ceram. Soc.,* 98[9] 2902-07 (2015).
3. N. Anantharamulu, K. K. Rao, G. Rambabu, B. V. Kumar, V. Radha, and M. Vithal, "A wide-ranging review on Nasicon type materials," *J. Mater. Sci.,* 46 2821-37 (2011).
4. Q. Ma, C.-L. Tsai, X.-K. Wei, M. Heggen, F. Tietz, and J. T. S. Irvine, "Room temperature demonstration of a sodium superionic conductor with grain conductivity in excess of 0.01 S cm^{-1} and its primary applications in symmetric battery cells," *J. Mater. Chem. A,* 7 7766 (2019).
5. S. Balagopal, T. Landro, S. Zecevic, D. Sutija, S. Elangovan, and A. Khandkar, "Selective sodium removal from aqueous waste streams with NaSicon ceramics," *Sep. Purif. Tech.,* 15 231-37 (1999).
6. N. Kim, S. Jeong, W. Go, and Y. Kim, "A Na^+ ion-selective desalination system utilizing a NASICON ceramic membrane " *Water Res.,* 215 118250 (2022).
7. X. Liang, B. Wang, Han Zhang, Q. Diao, B. Quan, and G. Lu, "Progress in NASICON-based mixed-potential type gas sensors," *Sensor Actuat. B Chem,* 187 522-32 (2013).
8. Q. Ma and F. Tietz, "Solid-State Electrolyte Materials for Sodium Batteries: Towards Practical Applications," *ChemElectroChem,* 7 2693-713 (2020).
9. P. Pirayesh, E. Jin, Y. Wang, and Y. Zhao, "Na metal anodes for liquid and solid-state Na batteries," *Energy Environ. Sci.,* 17 442-96 (2024).
10. L. J. Small, A. Eccleston, J. Lamb, A. C. Read, M. Robins, T. Meaders, D. Ingersoll, P. G. Clem, S. Bhavaraju, and E. D. Spoerke, "Next generation molten NaI batteries for grid scale energy storage," *J. Power Sources,* 360 569-74 (2017).
11. M. M. Gross, S. J. Percival, R. Y. Lee, A. S. Peretti, E. D. Spoerke, and L. J. Small, "A high-voltage, low-temperature molten sodium battery enabled by metal halide catholyte chemistry," *Cell Rep. Phys. Sci.,* 2 10489 (2021).
12. R. C. Hill, M. S. Gross, S. J. Percival, A. S. Peretti, L. J. Small, E. D. Spoerke, and Y.-T. Cheng, "Molten sodium batteries: advances in chemistries, electrolytes, and interfaces," *Front. Batt. Electrochem.,* 3 1369305 (2024).
13. A. M. Maraschky, M. L. Meyerson, S. J. Percival, D. R. Lowry, S. Meserole, J. N. Williard, A. S. Peretti, M. Gross, L. J. Small, and E. D. Spoerke, "Impact of Catholyte Lewis Acidity at the Molten Salt-NaSICON Interface in Low-Temperature Molten Sodium Batteries," *J. Phys. Chem. C,* 127 1293-302 (2023).
14. J. M. Weller, M. M. Li, E. Polikarpov, K. S. Han, N. Kidner, A. Patel, M. Nguyen, M. Stout, M. Gossett, K. Jung, D. M. Reed, V. L. Sprenkle, and G. Li, "Unlocking the NaCl-$AlCl_3$ phase diagram for low-cost, long-duration Na-Al batteries," *Energy Storage Mater.,* 56 108-20 (2023).
15. J. Oh, X. Xu, Z. Zeng, K. Wang, N. Tan, E. Kok, J. Huang, and L. Lu, "Thin NASICON Electrolyte to Realize High Energy Density Solid-State Sodium Metal Battery," *Energy Environ. Mater.,* 6 e12472 (2023).
16. A. Parejiya, M. Dixit, R. Essehli, R. Amin, and I. Belharouak, "Unleashing the Potential of NASICON Materials for Solid-State Batteries," *JOM,* 76[3] 1088-93 (2024).

17. M. Li, M. Dixit, R. Essehli, C. J. Jafta, R. Amin, M. Balasubramanian, and I. Belharouak, "$Na_3Zr_2Si_2PO_{12}$ Solid Electrolyte Membrane for High-Performance Seawater Battery," *Adv. Sci.,* 10[17] 2300920 (2023).
18. A. K. Kuriakose, T. A. Wheat, A. Ahamad, and J. Dirocco, "Synthesis, Sintering, and Microstructure of Nasicons," *J. Am. Ceram. Soc.,* 67[3] 179-83 (1984).
19. R. S. Gordon, G. R. Miller, B. J. McEntire, E. D. Beck, and J. R. Rasmussen, "Fabrication and Charaterization of NaSICON Electrolytes," *Solid State Ionics,* 3 234-48 (1981).
20. N. S. Bell, C. Edney, J. S. Wheeler, D. Ingersoll, and E. D. Spoerke, "The Influences of Excess Sodium on Low-Temperature NaSICON Synthesis," *J. Am. Ceram. Soc.,* 97 3744-48 (2014).
21. H. Perthuis and P. Colomban, "Sol-gel routes leading to nasicon ceramics," *Ceramics International,* 12[1] 39-52 (1986).
22. J.-S. Lee, C.-M. Chang, Y. I. Lee, J.-H. Lee, and S.-H. Hong, "Spark Plasma Sintering (SPS) of NASICON Ceramics," *J. Am. Ceram. Soc.,* 87 305-07 (2008).
23. J. G. P. d. Silva, M. Bram, A. M. Laptev, J. Gonzalez-Julian, Q. Ma, F. Tietz, and O. Guillon, "Sintering of a sodium-based NASICON electrolyte: A comparative study between cold, field assisted and conventional sintering methods," *J. Eur. Ceram. Soc.,* 39 2697-702 (2019).
24. M. Kimura, K.-T. Tseng, J. Wolfenstine, and J. Sakamoto, "The use of hot-pressing to reduce grain boundary resistance in Nasicon of nominal composition $Na_3Zr_2Si_2PO_{12}$," *Solid State Ionics,* 411 116561 (2024).
25. Y. B. Rao, K. K. Bharathi, and L. N. Patro, "Review on the synthesis and doping strategies in enhancing the Na ion conductivity of $Na_3Zr_2Si_2PO_{12}$ (NASICON) based solid electrolytes," *Solid State Ionics* 366-67 (2021).
26. D. Zuo, L. Yang, Z. Zou, S. Li, Y. Feng, S. J. Harris, S. Shi, and J. Wan, "Ultrafast Synthesis of NASICON Solid Electrolytes for Sodium-Metal Batteries," *Adv. Energy Mater.,* 13[37] 2301540 (2023).
27. S. Narayanana, S. Reid, S. Butler, and V. Thangadurai, "Sintering temperature, excess sodium, and phosphorous dependencies on morphology and ionic conductivity of NASICON $Na_3Zr_2Si_2PO_{12}$," *Solid State Ionics,* 331 22-29 (2019).
28. S. Kim, S. Shin, D. S. Jung, J. Chun, Y. C. Kang, and J. H. Kim, "Scalable Dry Process for Fabricating a Na Superionic Conductor-Type Solid Electrolyte Sheet," 16[8] 10307-15 (2024).
29. A. G. Jolley, G. Cohn, G. T. Hitz, and E. D. Wachsman, "Improving the ionic conductivity of NASICON through aliovalent cation substitution of $Na_3Zr_2Si_2PO_{12}$," *Ionics,* 21 3031-38 (2015).
30. M. Samiee, B. Radhakrishnan, Z. Rice, Z. Deng, Ying Shirley Meng, S. P. Ong, and J. Luo, "Divalent-doped $Na_3Zr_2Si_2PO_{12}$ natrium superionic conductor: Improving the ionic conductivity via simultaneously optimizing the phase and chemistry of the primary and secondary phases," *J. Power Sources,* 347 229-37 (2017).
31. X. G. Cao, X. H. Zhang, T. Taoa, and H. Y. Zhang, "Effects of antimony tin oxide (ATO) additive on the properties of $Na_3Zr_2Si_2PO_{12}$ ceramic electrolytes," *Ceramic International,* 46 8405-12 (2020).
32. M. Sozak, T. Nazarenus, J. Exner, J. Kita, and R. Moos, "Room temperature manufacture of dense NaSICON solid electrolyte films for all-solid-state-sodium batteries," *J. Mater. Sci.,* 58 10108-19 (2023).

33. Y. Xing, Y. Li, and C. Zhang, "Low temperature preparation of dense and highly conductive NASICON electrolyte by solid-state reactive sintering," *Solid State Ionics,* 373 115811 (2021).
34. M. Wu, H. Liu, X. Qi, D. Li, C. Wang, C.-W. Nan, and L.-Z. Fan, "Structure designing, interface engineering, and application prospects for sodium-ion inorganic solid electrolytes," *InfoMat,* 6 e12606 (2024).
35. J. Engell, S. Mortensen, and L. Møller, "Fabrication of Nasicon electrolytes from metal alkoxide derived gels," *Solid State Ionics,* 9-10 877-84 (1983).
36. J. Kim, S. H. Jo, S. Bhavaraju, A. Eccleston, and S. O. Kang, "Low temperature performance of sodium–nickel chloride batteries with NaSICON solid electrolyte," *J. Electroanal. Chem.,* 759 201-06 (2015).
37. J. T. S. Irvine, Derek C. Sinclair, and A. R. West, "Electroceramics: Characterization by Impedance Spectroscopy," *Adv. Mater.,* 2 132-38 (1990).
38. E. J. Cheng, T. Yang, Y. Liu, L. Chai, R. Garcia-Mendez, E. Kazyak, Z. Fu, G. Luo, F. Chen, R. Inada, V. Badilita, H. Duan, Z. Wang, J. Qin, H. Li, S.-i. Orimo, and H. Kato, "Correlation between mechanical properties and ionic conductivity of polycrystalline sodium superionic conductors: A relative density-dominant relationship," *Materials Today,* 44 101644 (2024).
39. M. Kizilyalli and A. J. E. Welch, "Preparation and X-Ray Powder Diffraction Data for Anhydrous Sodium Orthophosphates," *J. Inorg. Nucl. Chem.,* 38 1237-40 (1976).
40. B. J. McEntire, R. A. Bartlett, G. R. Miller, and R. S. Gordon, "Effect of Decomposition on the Densification and Properties of Nasicon Ceramic Electrolytes," *J. Am. Ceram. Soc.,* 66[10] 738-42 (1983).